



# CHORUS

This is the accepted manuscript made available via CHORUS. The article has been published as:

## Surface Polarization Effects on Ion-Containing Emulsions

Meng Shen, Honghao Li, and Monica Olvera de la Cruz

Phys. Rev. Lett. **119**, 138002 — Published 28 September 2017

DOI: [10.1103/PhysRevLett.119.138002](https://doi.org/10.1103/PhysRevLett.119.138002)

# Surface Polarization Effects on Ion-Containing Emulsions

Meng Shen,<sup>1</sup> Honghao Li,<sup>2</sup> and Monica Olvera de la Cruz<sup>1,2,\*</sup>

<sup>1</sup>*Department of Materials Science and Engineering, Northwestern University, Evanston, IL 60208*

<sup>2</sup>*Department of Applied Physics, Northwestern University, Evanston, IL 60208*

(Dated: September 5, 2017)

Surface polarization in ion-containing heterogeneous dielectric media such as cell media and emulsions is determined by and determines the positions of the ions. We compute the surface polarization self-consistently as the ions move and analyze their effects on the interactions between electro-neutral, ion-containing droplets using coarse-grained molecular dynamics simulations based on the true energy functional. For water droplets immersed in oil, the inter-droplet interaction is attractive, and the surface polarization makes the major contribution. By contrast, for oil droplets in water, the ion-surface induced charge interaction is repulsive and counteracts the attraction between the ions, leading to a small attractive interaction between the droplets. This research improves our understanding of self-assembly in mixed phases such as metal extraction for recovering rare earth elements and nuclear waste as well as water purification.

PACS numbers: 41.20.Cv, 77.84.Nh

Aggregation of foreign phases in dielectric media that contain ions is ubiquitous in biological systems, oil refining industry and water purification membranes [1–3]. Segregation of ion-containing emulsions in organic solvents is particularly important in extraction of rare earths and nuclear waste. In such processes, multivalent ions and their counterions are encapsulated in self-assembled nano-droplets of water immersed in oil. In the case of amphiphiles encapsulating electroneutral water droplets with trivalent ions (such as lanthanides) together with monovalent counterions in oil, for example, the droplets flocculate into clusters [4], and X-ray scattering data reveal long range inter-droplet interactions. A unique feature of these emulsions is the permittivity difference, which gives rise to surface polarization when there is a local electrical field either due to an external field or due to the presence of charges in the system. In order to understand the aggregation of ion-containing emulsions, it is important to study how the surface polarization contributes to the inter-droplet interactions.

In all-atom molecular dynamics (MD) simulations, polarization effects are included in the atomic details of the solvent molecules [5]. However, the role of surface polarization cannot be extracted from all-atom MD simulations. As a result, the role of the surface polarization in ion-containing aggregates has remained elusive. Therefore, coarse-grained MD simulations (CGMD) that include explicitly surface polarization effects are desired [6]. Recently, surface polarization has been introduced in implicit solvent CGMD using the boundary element method [7–9], perturbation theory [10] and the variational method [11, 12].

In this research, we use CGMD to investigate the role of surface polarization in the interaction between ion-containing electro-neutral droplets in heterogeneous dielectric media. In contrast to traditional CGMD, this work directly considers interfacial polarization by mini-

mizing the energy functional of surface induced charges [12]. This method agrees well with analytic results for the case of charged hard spheres [10] (see SI [18], **which includes Refs. [19–25]**). We first simulate two water droplets immersed in an oil medium, each droplet is 1 nm in diameter and encloses cations and anions with stoichiometric ratio (Fig. 1), consistent with the observation in all-atomistic simulations for metalloamphiphiles studies [4]. Constant and non-fluctuating spherical droplets are adopted since we are interested in the time-averaged interaction, and the inter-droplet correlations are observed to be stable up to tens of nanoseconds [4]. We then simulate the opposite case of two droplets with lower dielectric constant (oil) of the same dimensions immersed in water (Fig. 1) to determine the role of surface polarization in settings close to biological conditions such as interactions between bacterial micrompartments including carboxysomes [13]. Trivalent cations and monovalent anions of 2 Å radii are first studied, corresponding to  $\text{Eu}^{3+}$  and  $\text{NO}_3^-$  studied in experimental measurements [4], since only multivalent ions are pertinent for recovering rare earths and nuclear waste studies, and lanthanides are particularly important in these studies because only few of them are radioactive, which permits scientists to explore their physical properties safely. Then we vary the ion size and valency. We model ions explicitly, and we model solvents implicitly. We neglect surfaces [14] and confinement effects [15] on the permittivity of the media. We assume the bulk permittivity is 80 for water, and 5 for oil. A discontinuous jump in the permittivity of the implicit solvent is used to determine the effect of surface polarization without the need of including fitting parameters. However, the permittivity is lowered to account for the effect of salt on the medium permittivity [26] in the supplemental material (SM) [18]. Despite of several approximations in the model, our results of inter-droplet interaction en-

ergy closely match the experimental results by SAXS [4]. Four cases with droplet1/medium/droplet2 permittivity values ( $\epsilon_1/\epsilon_3/\epsilon_2$ ) are studied: (a) water droplets in oil (80/5/80), (b) oil droplets in water (5/80/5), (c) pure water (80/80/80) and (d) pure oil (5/5/5).

The role of surface polarization can be addressed starting from the definition of polarization vector  $\mathbf{P}(\mathbf{x}) = -\frac{[\epsilon(\mathbf{x})-1]\nabla\psi(\mathbf{x})}{4\pi}$ , where  $\epsilon(\mathbf{x})$  is permittivity, and  $\psi(\mathbf{x})$  is electrostatic potential. Gaussian units are used. However, polarization vector is a volume vector in a non-trivial dielectric medium, namely, it is non-zero wherever the electrical field is not zero, making the surface polarization contributions hard to separate from the total electrostatic interactions. In addition, surface polarization is dynamically entangled with the positions of real charges, therefore, it is rather difficult to be calculated and remains unresolved for decades. Fortunately, the induced charge density, which is defined as  $\rho_i(\mathbf{x}) = -\nabla \cdot \mathbf{P}(\mathbf{x})$ , vanishes except when  $\nabla\epsilon(\mathbf{x})$  or  $\rho_r(\mathbf{x})$  is not zero, where  $\rho_r(\mathbf{x})$  is real charge density, i.e. the induced charge is not zero only at dielectric interfaces or at the location of real charges. Therefore, the determination of induced charges enables the separation of surface polarization contributions from total electrostatic interactions.

We obtain the induced charges using a variational method based on the true energy functional of induced charges [12, 16]:

$$\begin{aligned} I[\omega] = & \frac{1}{2} \int_V \int_V \rho_r(\mathbf{x}) R_{\rho\rho}(\mathbf{x}, \mathbf{x}') \rho_r(\mathbf{x}') d^3\mathbf{x}' d^3\mathbf{x} \\ & + \frac{1}{2} \sum_k \int_V \int_{S_k} \rho_r(\mathbf{x}) R_{\rho\omega}(\mathbf{x}, \mathbf{x}_k) \omega(\mathbf{x}_k) d^2\mathbf{x}_k d^3\mathbf{x} \quad (1) \\ & + \frac{1}{2} \sum_{k,l} \int_{S_k} \int_{S_l} \omega(\mathbf{x}_k) R_{\omega\omega}(\mathbf{x}_k, \mathbf{x}_l) \omega(\mathbf{x}_l) d^2\mathbf{x}_l d^2\mathbf{x}_k \end{aligned}$$

where  $\omega$  is the surface induced charge density,  $k, l$  are indices that enumerate the interfaces, and  $R_{\rho\rho}$ ,  $R_{\rho\omega}$  and  $R_{\omega\omega}$  are Green's functions that take surface polarization into account as defined in SI [18].

Note Eq. (1) extends the formula of the energy functional from one interface [11] to multiple interfaces. We emphasize that Eq. (1) is a true energy functional of induced charges [12]. Minimizing Eq. (1) solves for the induced charges and gives the true electrostatic energy.

In our CGMD studies, surfaces are meshed into 0.0095 nm<sup>2</sup> triangular patches and the induced charges are obtained by minimizing the discretized energy functional. The electrostatic force on the ions is then calculated as the product of ion charge and the electrical field. The excluded volume of the ions is represented by a shifted repulsive Lennard-Jones potential:  $u_{LJ} = 4\epsilon[(\frac{\sigma}{r})^{12} - (\frac{\sigma}{r})^6] + \epsilon$  for  $r \leq 2\frac{1}{6}\sigma$ , where  $\epsilon$  and  $\sigma$  are the energy and distance parameter, respectively.  $\epsilon$  is 1  $k_B T$  and  $\sigma$  depends on the ion sizes. The encapsulation of the ions by the droplet surface is guaranteed by a shifted repul-

sive Lennard-Jones potential. The dynamics of ions is advanced following Newton's second law [17]. To simulate the constant temperature ensemble, the system is coupled to a Langevin thermostat at a temperature of 300 K. The timestep is 1 fs. All simulations are run for at least 10 ns.

The electrostatic energy can be separated into bulk and surface contributions using  $\omega(\mathbf{x}')$ , the surface induced charge density [11]. Integrating by parts the electrostatic energy  $U = \frac{1}{8\pi} \int_V \epsilon(\mathbf{x}) E^2(\mathbf{x}) d^3\mathbf{x}$  becomes  $U = \frac{1}{2} \int_V \rho_r(\mathbf{x}) \psi(\mathbf{x}) d^3\mathbf{x}$ , which contains the bulk charges and surface induced charges [18]:

$$\begin{aligned} U = & \frac{1}{2} \int_V \int_V \frac{\rho_r(\mathbf{x}) \rho_r(\mathbf{x}')}{\epsilon(\mathbf{x}') |\mathbf{x} - \mathbf{x}'|} d^3\mathbf{x}' d^3\mathbf{x} \\ & + \frac{1}{2} \int_V \int_S \frac{\rho_r(\mathbf{x}) \omega(\mathbf{x}')}{|\mathbf{x} - \mathbf{x}'|} d^2\mathbf{x}' d^3\mathbf{x} \quad (2) \end{aligned}$$

The first term is the electrostatic interactions excluding the surface charges, and the second term is the contribution that involves surface polarization. To be concise, we refer to the first term in Eq. (2) as ion-ion interactions, and the second term in Eq. (2) as ion-surface induced charge interactions. However, the factor of  $\frac{1}{2}$  in the second term indicates that this term contains not only real charge-induced charge interactions, but also induced charge-induced charge interactions.

It is known that surface polarization is determined by ion distribution, and surface polarization also affects ion distribution. The physics behind this intertwined relation is hardly understood without being able to separate the inter-droplet interactions into ion-ion interaction and ion-surface induced charge interaction. Fig. 1 shows the total, ion-ion and ion-surface induced charge interactions for the four cases (a) - (d). Fig. 1(a) shows that in case (a), the ion-surface induced charge interaction between the droplets contributes about 80% to the total inter-droplet electrostatic attraction at an inter-droplet distance of 11 Å. The total inter-droplet interaction is about 1.0  $k_B T$ , close to SAXS measurement in experiments [4]. The inter-droplet interaction is increased with decreasing permittivity inside the droplet, and the ion-surface induced charge interaction remains the major contribution (see SM [18]). The interaction energy decays with  $r^{-6}$ , where  $r$  is the distance between the two droplets (see fit curves in Fig. 1). This result shows that surface polarization enhances the inter-droplet attraction for water droplets in oil. To understand this enhancement, we notice that the surface induced charge adjacent to positive ions is positive, and vice versa, as is shown in the snapshot in the inset of Fig. 1(a) as well as the videos in SM [18]. That ions induce same sign charges can be understood by expanding in spherical harmonics induced

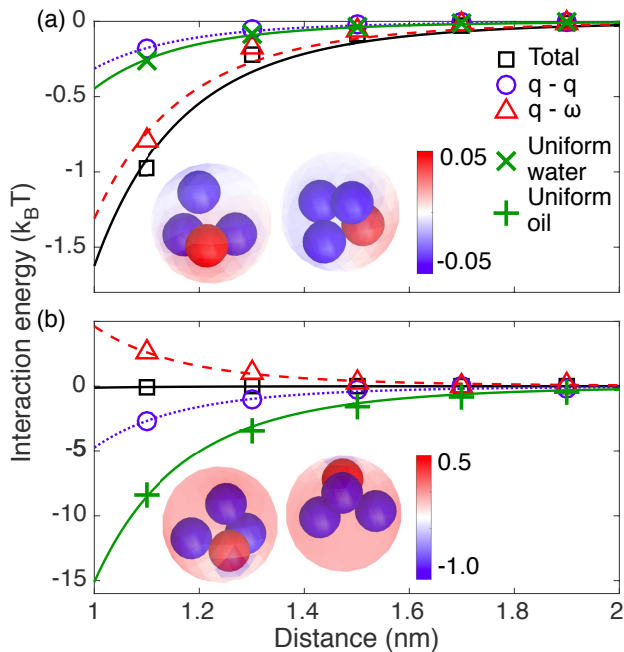


FIG. 1. Ion-ion (blue circles, fit in blue dotted lines), ion-induced charge (red triangles, fit in red dashed lines) and total (black squares, fit in solid black lines) inter-droplet interactions as a function of inter-droplet distance (a) between water droplets immersed in oil and (b) between oil droplets immersed in water. Inter-droplet interaction with uniform water permittivity (green crosses and fit in green solid lines in (a)) and with uniform oil permittivity (green pluses and fit in solid lines in (b)). Insets are snapshots of the simulations. Red means positive charges, and blue means negative charges. Videos are available in SM [18]. Color online.

charges in a single sphere,

$$\omega(R, \theta) = \frac{q(\epsilon_{in} - \epsilon_{out})}{4\pi\epsilon_{in}} \times \sum_{l=0}^{\infty} \frac{(l+1)(2l+1)d^l}{[l(\epsilon_{in} + \epsilon_{out}) + \epsilon_{out}]R^{l+2}} P_l(\cos\theta) \quad (3)$$

where  $\omega$  is the surface induced charge,  $q$  is the charge of an ion,  $R$  is the radius of the sphere,  $d$  is the distance from the ion to the center of the sphere,  $\theta$  is the polar angle,  $l$  is the order of each term in the expansion, and  $\epsilon_{in}$  and  $\epsilon_{out}$  is permittivity inside and outside the sphere, respectively. Eq. (3) shows that the induced charges are of the same sign as the ion inside the sphere when  $\epsilon_{in} > \epsilon_{out}$ . Consequently, the induced charges increase the total dipole moment formed by the real charges in each droplet, which enhances the inter-droplet attraction.

By contrast, in case (b), the ion-surface induced charge interaction between the droplets is repulsive, while the ion-ion interaction between the droplets is still attractive (Fig. 1(b)). These two types of interactions counteract each other, leading to a very small inter-droplet attraction (Fig. 1(b)). As shown in the inset in Fig. 1(b) and

the videos in SM [18], the surface induced charges are of the opposite sign as the charge of the ion adjacent to the interface grids, which cancels out the dipole moment formed by the ions within the droplet. This is consistent with the spherical harmonics expansion approximation in Eq. (3).

To reinforce the importance of including surface polarization for the inter-droplet interactions, we perform simulations without considering surface polarization, using uniform permittivity throughout the system and compare with simulations that consider surface polarization. Fig. 1(a) shows that when water permittivity is used throughout the system (case (c) shown in green crosses in Fig. 1(a)), the total inter-droplet interaction is close to the ion-ion interaction between the droplets for water droplets in oil. This is not surprising, considering that only ion-ion interaction exists for simulations with uniform permittivity, and the permittivity inside the droplets in the two cases is the same. This comparison also indicates that using uniform water permittivity underestimates the total inter-droplet interaction for water droplets in oil by a large amount when surface polarization is neglected. Moreover, by comparing case (a) (black squares in Fig. 1(a)) with case (d) (green plus signs in Fig. 1(b)), we find that simulations with uniform oil permittivity overestimates the inter-droplet interaction by an order of magnitude. We attribute this to the increased electrostatic interaction between ions due to decreased permittivity. The above comparisons indicates that the total inter-droplet interaction is not simply reproduced by arbitrarily choosing the permittivity inside or outside the droplets.

On the other hand, the comparison between case (b) (black squares in Fig. 1(b)) and case (d) (green plus signs in Fig. 1(b)) shows that when uniform oil permittivity is used, the total inter-droplet attraction is overestimated for oil droplets in water. Moreover, uniform water permittivity in case (c) also overestimates the total inter-droplet interaction for oil droplets in water.

It is interesting that the inter-droplet interaction for case (d) with uniform oil permittivity is at least twice the inter-droplet ion-ion interaction for oil droplets in water in case (b) (Fig. 1(b)). This seems inconsistent with the fact that the permittivity inside the the droplets is the same for the two cases, which seems to correspond to similar ion-ion interactions between the droplets for the two cases, based on Eq. (2). To understand this difference in ion-ion interactions with or without accounting for surface polarization, we recall that surface polarization not only is determined by the ion distribution, but also determines the ion distribution, and consequently ion-ion inter-droplet interactions. The effect of surface polarization on the ion-ion inter-droplet interaction can be analyzed with dipole-dipole interactions by simply modeling

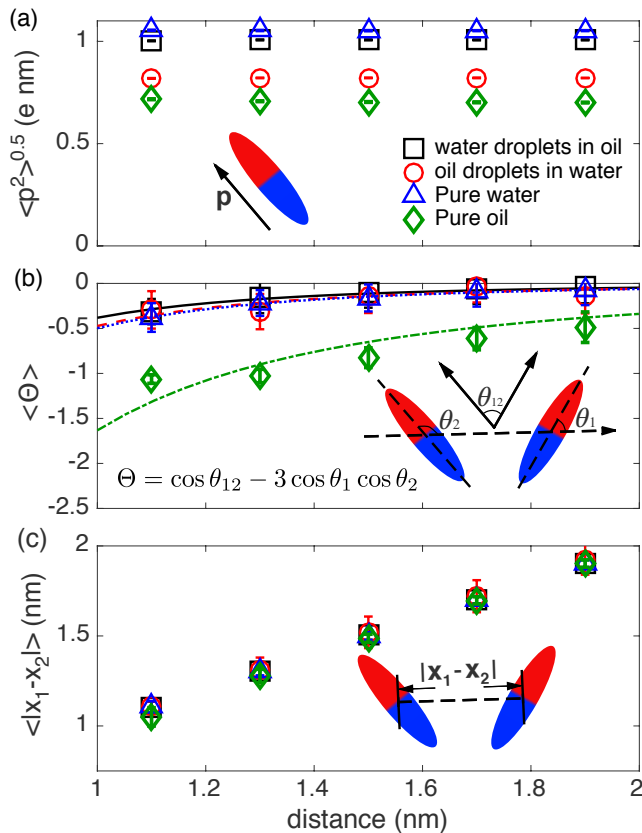


FIG. 2. (a) the average magnitude of dipole moment, (b) the orientation factor between dipoles and (c) the distance between the center of dipoles formed by ions in each droplet for water droplets in oil (black squares), oil droplets in water (red circles), uniform water permittivity (blue triangles) and uniform oil permittivity (green diamonds). Color online.

ions in each droplet as one dipole:

$$W = \frac{|\mathbf{p}(\mathbf{x}_1)| |\mathbf{p}(\mathbf{x}_2)| (\cos \theta_{12} - 3 \cos \theta_1 \cos \theta_2)}{\epsilon |\mathbf{x}_1 - \mathbf{x}_2|^3} \quad (4)$$

where  $W$  is the interaction energy between dipoles  $\mathbf{p}(\mathbf{x}_1)$  and  $\mathbf{p}(\mathbf{x}_2)$ ,  $\theta_{12}$  is the angle between the two dipoles,  $\theta_1$  ( $\theta_2$ ) is the polar angle of dipole 1 (dipole 2) with respect to  $\mathbf{n}$ , the unit vector in the direction of  $(\mathbf{x}_1 - \mathbf{x}_2)$ , and  $\epsilon$  is permittivity where the dipoles are.

Based on Eq. (4), the ion-ion interaction between the droplets is determined by four factors in the framework of dipole-dipole interactions: i) the magnitude of the dipoles,  $|\mathbf{p}(\mathbf{x}_1)|$  and  $|\mathbf{p}(\mathbf{x}_2)|$ , ii) the orientation factor of the dipoles  $\Theta = \cos \theta_{12} - 3 \cos \theta_1 \cos \theta_2$ , iii) the distance between the dipoles,  $|\mathbf{x}_1 - \mathbf{x}_2|$ , and iv) the permittivity  $\epsilon$ . While the factor iv) is an input to CGMD, the rest of the factors vary upon ion distribution within the droplets, and are shown in Fig. 2 for all four cases (a) to (d).

The average magnitude of the dipole moment formed by ions in each droplet  $\sqrt{\langle \mathbf{p}^2 \rangle}$  is smaller in cases (b)

and (d) than cases (a) and (c), as shown in Fig. 2(a), because the electrostatic attraction between ions is stronger in oil than in water, leading to smaller cation-anion distances. Moreover,  $\sqrt{\langle \mathbf{p}^2 \rangle}$  is smaller for water droplets in oil (case (a)) than in uniform water permittivity (case (c)), because ions inside droplets induce surface-induced charges of the same sign, which repel the ions from the surface, making cation-anion distances even smaller. On the contrary,  $\sqrt{\langle \mathbf{p}^2 \rangle}$  is larger for oil droplets in water (case (b)) than in uniform oil permittivity (case (d)), because ions inside droplets induce opposite-sign surface induced charges, pulling ions towards the surfaces.

Fig. 2(b) shows that the orientation factor,  $\Theta$ , is much more negative for uniform oil permittivity (case (d)) than the other cases, which has the strongest total inter-droplet attraction in Fig. 1. The dipoles are oriented to minimize the enthalpic driven free energy for case (d). We note that  $\Theta$  is 0 for fully random orientations. For cases (a) and (c), the ion-ion electrostatic interactions are normalized by large permittivities, making enthalpic contribution to the free energy less pronounced. Therefore, the dipoles formed by ions in each droplet are more randomly oriented to maximize the entropy. For case (b), the ion-ion attraction between the droplets is canceled out by surface polarization, leading to little enthalpic contribution to the total free energy, therefore, the orientation dependence of the free energy for case (b) is weakened, also leading to random orientations.

The energy functional based CGMD and the separation of inter-droplet interaction enables to understand the physics behind the observed phenomena. The difference in the magnitude and the orientation factor of the dipole moments formed by the ions in each droplet for cases (a) to (d) show that the surface polarization and ion distribution are inter-dependent. Moreover, the average distance between the center of dipoles is more or less of the same length scale as the distance between the droplets. We note that strictly speaking, ion-ion inter-droplet interactions not only include dipoles but also quadruples, which are important for short-range inter-droplet interactions, but their contribution decays sharply with the inter-droplet distance.

Using explicit calculation of induced charges and separation of electrostatic inter-droplet interaction, our work provides a clear understanding behind the intertwined relation between surface polarization and ion distribution. Besides finding strong attractions between droplets with multivalent ions in agreement with all-atom metalloamphiphile extraction studies [4], we find the orientation of the charges in the droplets is strongly affected by the surface polarization and hence the ion-ion interaction between the droplets; these interactions decrease as the ion size and valency decreases (see SM [18]). Our studies reveal the role of dielectric mismatch on inter-droplet interactions. While ion-containing oil aggregates in aqueous solutions interact very weakly with each other,

much weaker than in the case of simulations that do not include surface polarization, in organic solvents the interactions between water droplets are strongly enhanced due to surface polarization. For the successful recovery of rare earths and nuclear waste, the ion containing droplets need to be dispersed in the oil phase. Our studies show that the attraction strength increases as the permittivity inside the droplets decreases [18]. Therefore, dispersion can be optimized by forming larger droplets which should have lower concentration of ions and therefore a lesser decrease of water permittivity [26] and/or by selecting oils with a higher dielectric constant. This understanding helps building meaningful models for analyzing interactions between ion containing emulsions and micro-compartments [27], and paves the way for understanding self-assembly of mixed phases for multiple applications.

We thank Baofu Qiao, Mykola Tasinkevych, Kyle Q. Hoffmann, Martin Girard and Chase Brisbois for useful discussions and MICCoM for financial support of the the U.S. Department of Energy, via grant #3J-30081-0056A//3J-30081-0056B.

---

\* Corresponding author:

m-olvera@northwestern.edu

- [1] D. E. Clapham, *Cell* **131**, 1047, (2007).
- [2] S. Ogawa, E. A. Decker, and D. J. McClements, *J. Agric. Food Chem.* **51**, 5522 (2003).
- [3] D. Gauthier, P. Baillargeon, M. Drouin, and Y. L. Dory, *Angew. Chem. Int. Ed.* **40**, 4635 (2001).
- [4] B. Qiao, G. Ferru, M. O. de la Cruz, and R. J. Ellis, *ACS Cent. Sci.* **1**, 493 (2015).
- [5] N. F. A. Van Der Vegt, K. Haldrup, S. Roke, J. Zheng, M. Lund, and H. J. Bakker, *Chem. Rev.* **116**, 7626 (2015).
- [6] J. Rottler and A.C. Maggs, *Phys. Rev. Lett.* **93**, 170201 (2004).
- [7] K. Barros and E. Luijten, *Phys. Rev. Lett.* **113**, 017801 (2014).
- [8] K. Barros, D. Sinkovits, and E. Luijten, *J. Chem. Phys.* **140**, 064903 (2014).
- [9] X. Jiang, J. Li, X. Zhao, J. Qin, D. Karpeev, J. Hernandez-Ortiz, J. J. de Pablo, and O. Heinonen, *J. Chem. Phys.* **145**, 064307 (2016).
- [10] J. Qin, J. Li, V. Lee, H. Jaeger, J. J. de Pablo, and K. F. Freed, *J. Colloid Interface Sci.* **469**, 237 (2016).
- [11] V. Jadhao, F. J. Solis, and M. O. de la Cruz, *Phys. Rev. Lett.* **109**, 223905 (2012).
- [12] V. Jadhao, F. J. Solis, and M. O. de La Cruz, *J. Chem. Phys.* **138**, 054119 (2013).
- [13] E. Y. Kim and D. Tullman-Ercek, *Biotechnol. J.* **9**, 348 (2014).
- [14] C. Zhang, F. Gygi, and G. Galli, *J. Phys. Chem. Lett.* **4**, 2477 (2013).
- [15] N. Giovambattista, P. J. Rossky, and P. G. Debenedetti, *Phys. Rev. E* **73**, 041604 (2006).
- [16] F. J. Solis, V. Jadhao, and M. O. de La Cruz, *Phys. Rev. E* **88**, 053306 (2013).
- [17] M. P. Allen and D. J. Tildesley, *Computer Simulation of Liquids* (Oxford University Press, New York, 1989).
- [18] See Supplemental Material at [URL will be inserted by publisher] for the simulation procedure, the derivation of electrostatic potential and energy with respect to the induced charges, the ion size and valence effects, the permittivity effects, the comparison with published analytical data and the videos of the trajectory of the ions and the induced charges.
- [19] W. C. Swope, H. C. Andersen, and P. H. Berens and K. R. Wilson, *J. Chem. Phys.* **76**, 637 (1982).
- [20] K. E. Gutowski, B. Gurkan, and E. J. Maginn, *Pure Appl. Chem.* **81**, 1799 (2009).
- [21] P. Salvador, J. E. Curtis, D. J. Tobias, and P. Jungwirth, *Phys. Chem. Chem. Phys.* **5**, 3752 (2003).
- [22] H. J. C. Berendsen, J. R. Grigera, and T. P. Straatsma, *J. Phys. Chem.* **91**, 6269 (1987).
- [23] K. P. Jensen, and W. L. Jorgensen, *J. Chem. Theory Comput.* **2**, 1499 (2006).
- [24] M. Neumann, O. Steinhauser, and G. S. Pawley, *Mol. Phys.* **52**, 97 (1984).
- [25] M. J. Abraham, and T. Murtola, and R. Schulz, S. Páll, J. C. Smith, B. Hess, and E. Lindahl, *SoftwareX* **1**, 19 (2015).
- [26] B. Hess, C. Holm, and N. van der Vegt, *Phys. Rev. Lett.* **96**, 147801 (2006).
- [27] T. O. Yeates, C. A. Kerfeld, S. Heinhorst, G. C. Cannon, and J. M. Shively, *Nature Rev. Microbiol.* **6**, 681 (2008).